Hindawi
Shock and Vibration
Volume 2018, Article ID 5319460, 13 pages
https://doi.org/10.1155/2018/5319460

*Research Article*

# Source Contribution Analysis for Exterior Noise of a High-Speed Train: Experiments and Simulations

**Jie Zhang, Xinbiao Xiao, Dewei Wang, Yan Yang, and Jing Fan**

*State Key Laboratory of Traction Power, Southwest Jiaotong University, Chengdu 610031, China*

Correspondence should be addressed to Xinbiao Xiao; xinbiaoxiao@163.com

Received 25 July 2018; Revised 26 September 2018; Accepted 13 November 2018; Published 5 December 2018

Academic Editor: Marco Tarabini



This paper presents a detailed investigation into the contributions of different sound sources to the exterior noise of a high-speed train both experimentally and by simulations. The in situ exterior noise measurements of the high-speed train, including pass-by noise and noise source identification, are carried out on a viaduct. Pass-by noise characteristics, noise source localizations, noise source contributions of different regions, and noise source vertical distributions are considered in the data analysis, and it is shown how they are affected by the train speed. An exterior noise simulation model of the high-speed train is established based on the method of ray acoustics, and the inputs come from the array measurements. The predicted results are generally in good agreement with the measurements. The results show that for the high-speed train investigated in this paper, the sources with the highest levels are located at bogie and pantograph regions. The contributions of the noise sources in the carbody region on the pass-by noise increase with an increasing distance, while those in the bogie and train head decrease. The source contribution rates of the bogie and the lower region decrease with increasing train speed, while those of the coach centre increase. At a distance of 25 m, the effect of the different sound sources control on the pass-by noise is analysed, namely, the lower region, bogie, coach centre, roof region, and pantograph. This study can provide a basis for exterior noise control of high-speed trains.

## 1. Introduction

The exterior noise of high-speed trains is an important problem influencing the living environment of citizens along high-speed railways. Therefore, effective control of exterior noise is a significant issue in the development of high-speed trains [1, 2]. Over the past decades, many research studies have been performed to determine the noise source characteristics of high-speed trains. Within Deutsche Bahn "Low Noise Railway" programme, a spiral microphone array was developed and used to investigate wheel and rail noise from a high-speed train [3]. Wakabayashi et al. [4] used a spiral microphone array to identify sound sources of a Shinkansen high-speed train (FASTECH360S). They found higher noise was generated from wheels. Poisson et al. [5] carried out noise source identification for TGV trains and found that the contribution of the rolling noise remains important at more than 300 km/h. Mellet et al. [6] investigated the contribution of aerodynamic/rolling noise for high-speed trains. They concluded that whether rolling noise is the most important source depends not only on the train speed but also on the wheel/rail surface conditions. Nagakura [7] performed wind tunnel tests using a 1/5 scale Shinkansen train model and analysed the distribution of aerodynamic noise sources. One of the conclusions was that the noise source at the front bogie of the leading car is much stronger than that at other bogies. He et al. [8] investigated the external noise of a high-speed train at different speeds and found that the rolling noise has a greater contribution to the total noise than the aerodynamic noise. Noh [9] used a microphone array to identify the noise sources of a high-speed train and found that the main noise sources are the intercoach spacing, wheels, and pantograph, when the train is running at 390 km/h. The different conclusions are related to the different vehicle types, track types, and train speeds in their studies.

In terms of using theoretical models, Talotte et al. [10] introduced the railway source models based on their physical parameters proposed in Harmonoise and presented how the database is organized and linked. For wheel/rail rolling noise, Remington [11] and Thompson and Gautier

[12] conducted comprehensive research studies on its mechanisms and predictions. Zea et al. [13] introduced a wavenumber-domain filtering technique, referred to as wave signature extraction, to separate the rail contribution to the total pass-by noise. Thompson et al. [14] assessed existing and new methods for rolling noise separation, including the wave signature extraction method, the beamforming method, the TWINS model with measured track vibration, the advanced transfer path analysis method, the MISO method, and the pass-by analysis method. It was found that most of these methods could obtain the track component of noise with acceptable accuracy. For aerodynamic noise, Latorre Iglesias et al. [15] proposed a semiempirical component-based prediction model to predict the aerodynamic noise from train pantographs. Zhu et al. [16] investigated the aerodynamic and aeroacoustic behaviour of the flow past a high-speed train wheelset which used a two-stage hybrid method of computational fluid dynamics and acoustic analogy. It was found that the radiated tonal noise corresponded to the dominant frequencies of the oscillating lift and drag forces from the wheelset.

In summary, significant research studies have been made into noise sources of high-speed trains. However, for exterior noise control of high-speed trains, attention should be given to both noise source identification and source contribution analysis. There are still few studies on the contribution analysis. This paper presents a detailed investigation into the contributions of different sound sources to the exterior noise of a high-speed train through experiments and simulations. In Section 2, the exterior noise measurement including pass-by noise and noise source identification of a high-speed train are introduced. In Section 3, the measurement results of pass-by noise, noise source localization, source contributions of different regions, and source vertical distributions are analysed. In Section 4, the exterior noise simulation model of the high-speed train is established, and the predicted results are verified by experiments. Finally, in Section 5, the contribution of the exterior noise sources to the pass-by noise is analysed including the influences of different train speeds and different source regions.

## 2. Exterior Noise Measurement of a High-Speed Train

*2.1. Pass-By Noise Measurement.* Figure 1 shows the measurement of the pass-by noise of a high-speed train. The measurement points are arranged according to the international standard ISO 3095 [17]. The two microphones were located at distances of 7.5 m and 25 m from the centreline of the track, respectively, and both at a height of 3.5 m above the upper surface of the rail.

The measured high-speed train consists of eight coaches. The first, the third, the sixth, and the last coaches are trailer car, while the other coaches are motor car. The length, the width, and the height (from railhead and not including the pantograph) of the train are, respectively, 209 m, 3.36 m, and 4.05 m. It was a new train, and the measurement was carried out on a testing line. Therefore, the wheel roughness and the rail roughness were both at low level. There is slab track on the viaduct using UIC 60 rail and WJ-8A fastening. For the slab track, the pad stiffness (the static stiffness) is around 20–30 kN/mm and the sleeper spacing is 0.625 m. The sidewall height is about 0.68 m relative to the bridge deck. The pass-by noise measurement was conducted using a B&K PULSE platform and 32768 Hz sampling frequency. All transducers were calibrated before the measurement.

*2.2. Noise Source Identification.* Figure 2 shows the measurement of the exterior noise source identification of the high-speed train, conducted using a 78-channel wheel microphone array (B&K WA-0890-F). The diameter of the array is 4 m, and the array centre was 7.5 m away from the centreline of the track and 2 m above the rail surface.

The exterior noise source identification was also conducted using a B&K PULSE platform and 16384 Hz sampling frequency. All transducers were calibrated before the measurement. The software B&K NSI array acoustics postprocessing was used for the exterior noise source identification analysis. The focus points are all set to be in the plane of the sidewall which is 5.8 m from the microphone array. The method is called rail vehicle moving source beamforming (BZ-5939) [18–21]. Table 1 shows the parameters used in the calculation.

## 3. Analysis on Characteristics and Contribution of Exterior Noise

*3.1. Pass-By Noise Analysis.* Figure 3 shows the A-weighted sound pressure level measured at pass-by when the train was running at 350 km/h.

It can be seen that the time-history curve of the sound pressure level at a distance of 7.5 m is more related to the train structure than that at a distance of 25 m. There are nine sound pressure peaks during a single pass-by at 350 km/h. The first peak corresponds to the entrance of the train head, while the last peak is attributed to the exit of the train tail. The other seven peaks between them represent the seven gaps among the eight coaches. The number of the curve valleys is equal to the number of coaches. It should be noted that the highest sound pressure level occurs at the first and second intercoach regions. During the pass-by time, the sound pressure levels decrease from the first intercoach to the train tail. For all the motor cars or trailer cars, they have the same wheel/rail rolling noise. This is attributed to, for different coaches of the high-speed train, the high aerodynamic noise levels at the front coach, while low aerodynamic noise levels occur at the end coach. This will be demonstrated in the next section using beamforming results.

The A-weighted equivalent continuous sound pressure levels ($L_{\mathrm{Aeq,Tp}}$) at the distances of 7.5 m and 25 m during the pass-by time are 101.0 dBA and 93.3 dBA, respectively. There is a 7.7 dBA reduction from 7.5 m to 25 m. The change for point sources obeying the inverse square law $20 \times \log_{10}(1/R)$ would be 10.5 dB, whereas for a line source, the change would be $10 \times \log_{10}(1/R)$ which is 5.3 dB. Hence the 7.7 dBA reduction observed may be due to the changing balance of line sources and point sources.

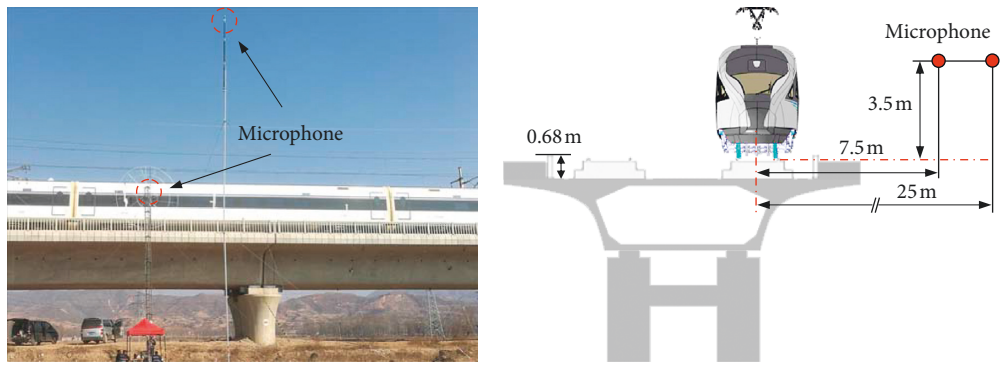


(a) (b)

Figure 1: Pass-by noise measurement of a high-speed train. (a) Measurement photograph. (b) Measurement points.

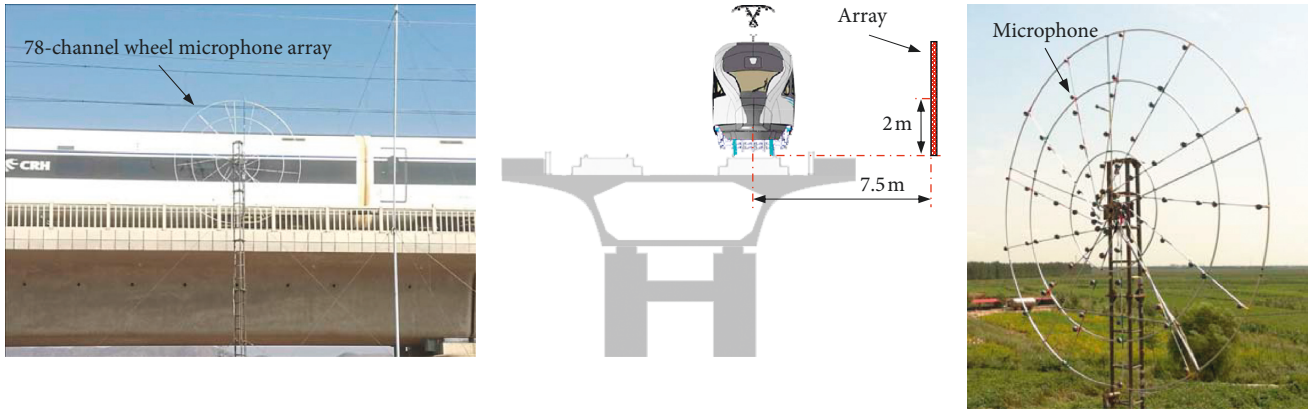


(a) (b) (c)

Figure 2: Noise source identification of a high-speed train. (a) Measurement photograph. (b) Measurement points. (c) 78-channel wheel microphone array (B&K WA-0890-F).

Figure 4 shows the frequency characteristics of the pass-by noise at the two different measurement points for the train running at 350 km/h.

As shown in Figure 4, for the measured points at distances 7.5 m or 25 m, the pass-by noise is dominated by high frequency components, especially in the 1/3 octave bands centred above 500 Hz. However, the sound pressure levels at high frequencies decrease at a higher rate with the increasing distance than those at low frequencies. In the 1/3 octave bands centred below 500 Hz, the sound pressure levels decrease by 5.0 dBA on average, between the two distances. Meanwhile, in the 1/3 octave bands centred above 500 Hz, the sound pressure levels decrease by 8.5 dBA on average. It is mainly due to the wavelength-dependent directivity of the acoustic waves.

According to the relationship between the exterior noise levels and speed of high-speed trains [6], when the value of $L_{\mathrm{Aeq,Tp}}(v_0)$ at the reference speed $v_0$ is known, a linear regression law can be expressed as

$$L_{\mathrm{Aeq,Tp}}(v) = a \log_{10}\left(\frac{v}{v_0}\right) + L_{\mathrm{Aeq,Tp}}(v_0), \quad (1)$$

where $a$ is a coefficient and $v$ is the train speed. The linear regressions for the two different measurement positions between the pass-by noise and the train speed are obtained from Equation (1).

Figure 5 shows the measured $L_{\mathrm{Aeq,Tp}}$ of the pass-by noise at different train speeds (it is always the same train). The horizontal axis represents train speed in the logarithmic scale.

It can be seen from Figure 5 that when the high-speed train is running with a speed in the 200–350 km/h range, the pass-by noise regression coefficients (i.e., $a$ in Equation (1)) for the two measurement positions at distances of 7.5 and 25 m are 29.5 and 28.5, respectively, with corresponding correlation coefficients $R^2 = 0.97$ for both distances. For the two measurement points, the regression coefficients are close to 30, which is commonly used in the prediction formula for wheel/rail rolling noise [6]. Hence, although different coaches suffer different aerodynamic noises, the rolling noise appears to be dominant for the whole train or for the pass-by time for a speed close to 350 km/h.

Furthermore, the difference of the pass-by noise level between the two measurement points can be written as

$$\Delta L_{\mathrm{p12}}(v) = \log_{10}\left(\frac{v}{v_0}\right) + 7.2. \quad (2)$$

Over the speed range of Figure 5, the difference between the regression lines changes by 0.24 dB. There is, therefore,

Table 1: The parameters used in the calculation.

| Weighting | Array shading | Array opening angle | Diagonal removal | Upsampling factor | Number of iterations | Deconvolution smoothing |
|---|---|---|---|---|---|---|
| A-weighted | Outdoor | 60° | No | x16 | 100 | Yes |

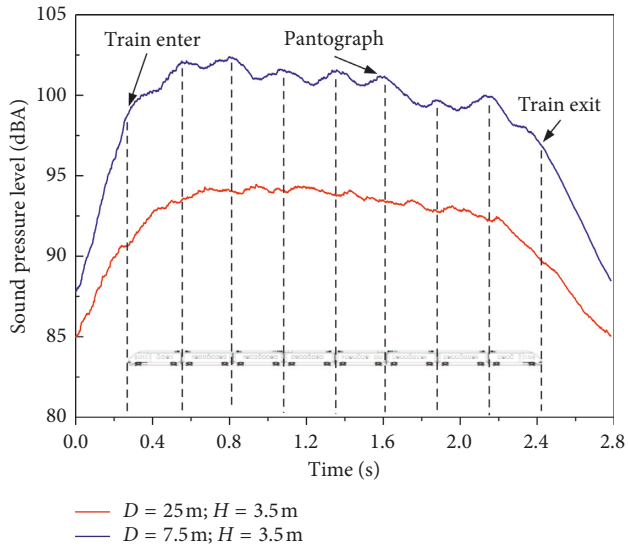


Figure 3: Time histories of the pass-by noise at different measurement points (350 km/h).

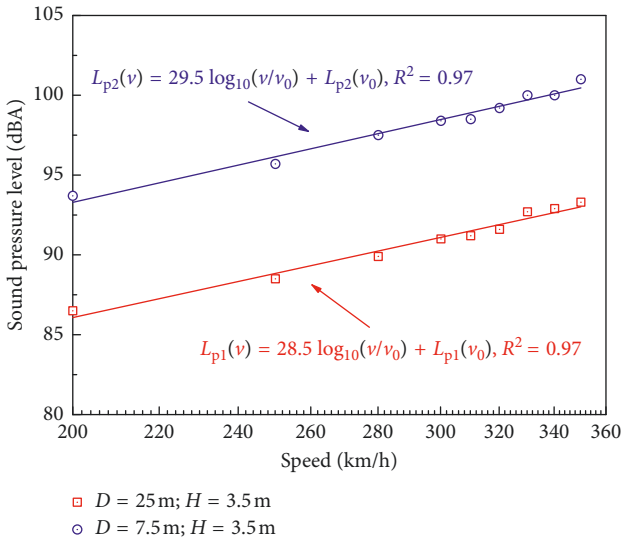


Figure 5: $L_{Aeq,Tp}$ results of the pass-by noise at different speeds.

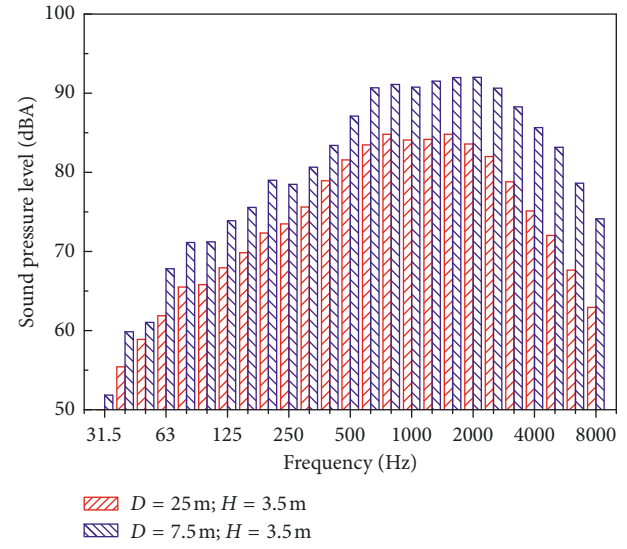


Figure 4: Frequency characteristics of the pass-by noise at different measurement points (350 km/h).

negligible difference between the speed dependence at the two distances.

*3.2. Noise Source Localization.* Figure 6 illustrates the distribution of the exterior noise sources of a high-speed train running at 350 km/h. As indicated above, the rail vehicle moving source beamforming method is used for postprocessing.

From Figure 6, when the high-speed train is running at 350 km/h, the sources with the highest levels are located at bogie and pantograph regions. The noise generated from the bogie includes the wheel/rail rolling noise, gear noise, and bogie aerodynamic noise. Rolling noise is generated by the interaction of the wheel and rail at their contact area, gear engagement produces gear noise, and aerodynamic noise is caused by the flow of air over the train as it travels at high speed. It can be seen that the sound intensity levels of different bogies are quite different. The noise levels decrease from the first to the last bogie. As indicated above, because the rolling noise level and gear noise level can be regarded to be approximately the same in each bogie, the main cause of the noise difference between different bogies should be the aerodynamic noise. For bogies located at different positions of the train, aerodynamic noise plays an important role, especially in the regions of the first five bogies (for trains running at high speed, such as 350 km/h).

*3.3. Contribution to the Total Sound Power from Different Regions of the Train.* The side surface of the high-speed train is divided into eight regions, as shown in Figure 7: bogie, pantograph, train head, train rear, intercoach, roof region, coach centre, and lower region.

The sound power is then obtained by integrating the sound intensity over each area, with each contribution calculated by using

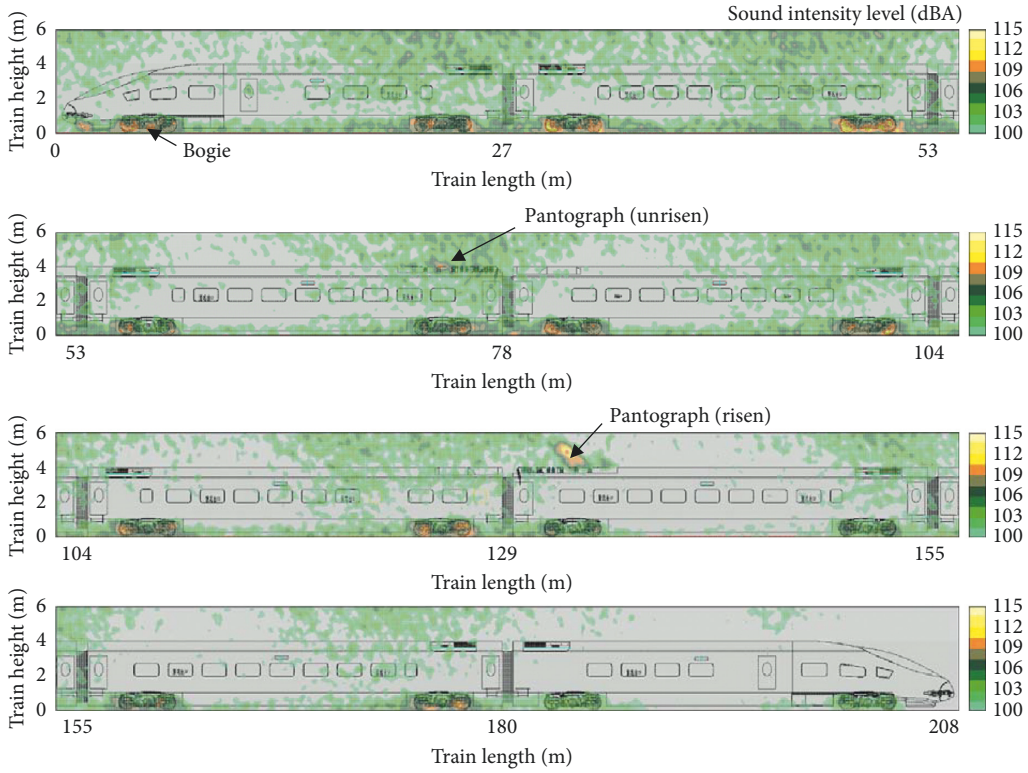


Figure 6: Exterior noise source distribution of the high-speed train running at 350 km/h (500–5000 Hz).

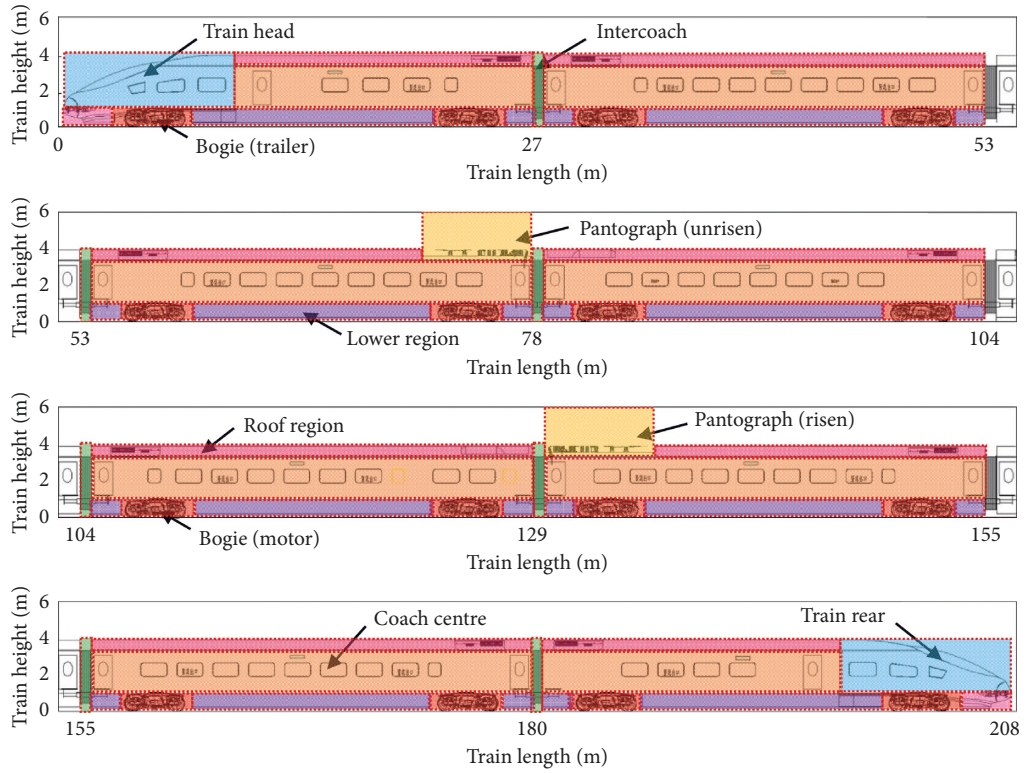


Figure 7: Divided regions of the entire high-speed train.

$$C_s = \frac{\int_{\Delta S} I(s)\, ds}{\int_S I(s)\, ds}, \quad (3)$$

where $I(s)$ is the sound intensity at a discrete point, $\Delta S$ is the area of each zone, and $S$ is the total area of all zones.

Because the resolution of the microphone array using the deconvolution algorithm is 15 dB, values of sound intensity level which are more than 15 dB lower than the maximum were set to 0 dB in order to avoid the influence of spurious sources on the calculation of sound power. However, from Figure 6, there may be still some spurious sources on the coach sides. In other words, source contribution from the carbody may be overestimated. Moreover, since the beamforming map is mainly concerned with the train itself, source contribution from the rail may be underestimated. These all should be further studied in the future.

Figure 8 shows the contribution rate of different regions to the total sound power.

It can be seen form Figure 8 that when the high-speed train runs at 350 km/h, the contribution rate of the bogie, coach centre, and lower region is relatively high, reaching 31.8%, 26.1%, and 21.1%, respectively. The contribution rate of the train head and intercoach is almost equal at 2.4% and 2.8%, respectively. The train rear shows the lowest contribution rate, with only 0.1%. Although the source with one of the highest levels is located at pantograph region, as indicated in Figure 6, its contribution is not very large because the high sound level only occupies small area, resulting in a low contribution.

Figure 9 shows sound power levels of exterior sources in different regions and the contribution rates of the sources at different speeds.

As shown in Figure 9(a), the sound power levels of most exterior sources increase with the increasing train speed, except for the sources in the train head and train rear. The sources in these two regions fluctuate according to the train speed. Furthermore, the law of contribution rates, as indicated in Figure 9(b), is quite different from that of the exterior source characteristics shown in Figure 9(a). The contribution rates of the three most significant exterior noise source regions, namely, the bogie, coach centre, and lower region, change with the train speed. The sound power contribution rates of both the bogie and lower region decrease as the speed increases. However, the sound power contribution rate of the coach centre increases with increasing speed. This is because the coach centre has the largest area, making it get more sound power including some spurious sources. The sound power contribution rates of the other regions are less than 10% and independent of the train speed. The sound power contributions of the pantograph and train head increase a little with the increasing speed, while those of the train rear decrease a little.

*3.4. Vertical Distribution of the Noise Sources of the Train.* The vertical distribution of the sound sources of the high-speed train expresses the intensity of the sound sources in the vertical direction and can be expressed through the single event sound level (SEL), given as

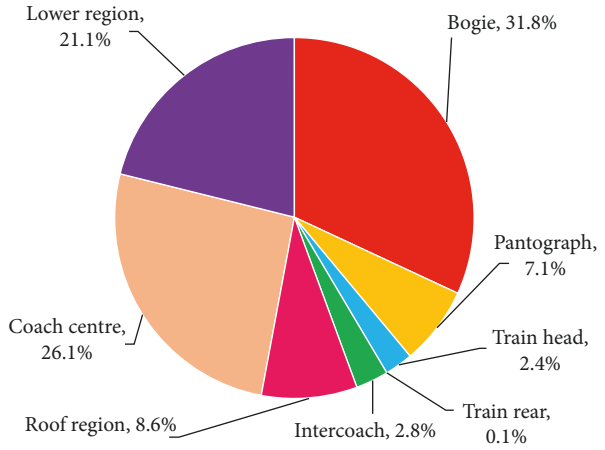


Figure 8: Contribution rate of the exterior sound sources to the total sound power (350 km/h).

$$\mathrm{SEL} = 10 \times \log_{10}\left(\int_l \frac{I(l)}{I_{\mathrm{ref}}}\, dl\right), \quad (4)$$

where $l$ is the length of the train, $I(l)$ is the sound intensity in the horizontal direction of the carbody, and $I_{\mathrm{ref}}$ is the reference sound intensity, equal to 1 pW/m$^2$. The area of the exterior noise source distribution of the high-speed train (as indicated in Figure 7) was 208 m in length and 6 m in height. The grid step was selected as 0.1 m. Hence, Equation (4) is the sound intensity integration in the horizontal direction of the beamforming acoustic map.

Figure 10 shows the vertical distribution of the exterior noise sources of a high-speed train running at 350 km/h.

When the high-speed train is running at 350 km/h, the maximum sound intensity level in the vertical direction is 128.1 dBA, at a height of 0.2 m above the railhead. The minimum sound intensity level of 118.1 dBA corresponds to a height of 1.4 m. Their height difference is 1.2 m, while their sound intensity level difference is 10 dBA. For heights in the 1.4–5.8 m range, the sound intensity level increases with increasing height. It is noteworthy that the sound intensity level tends to decrease at heights above 5.8 m. This may be related to the sound radiation directivity of the pantograph noise and also because there is no source higher than 5.8 m on the train. During the pass-by time, the sound intensity level in the vertical distribution is maximum in the bogie, followed by the lower region, pantograph, roof region, and coach centre. This order is somewhat different from the chart of relative contribution rates of different sources to the total sound power shown in Figure 8. The reason is mainly the way in which we divide the coach region. For example, in Figure 10, the pantograph region covers the entire length of the train; however, in Figure 8, the pantograph region covers the train area only partially.

Figure 11 shows the frequency distributions and frequency contribution rates of the exterior noise sources in the

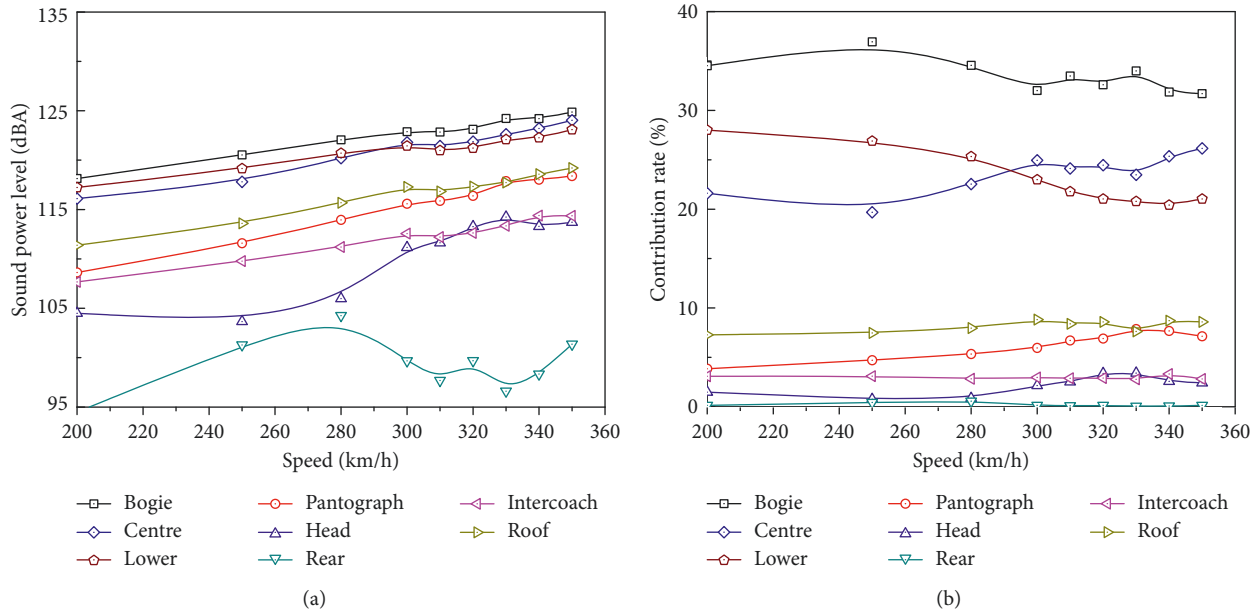


Figure 9: Exterior sound sources' characteristics and their contribution rates at different speeds. (a) Sound power levels of exterior sources in different regions. (b) Contribution rates of the exterior sources to total sound power.

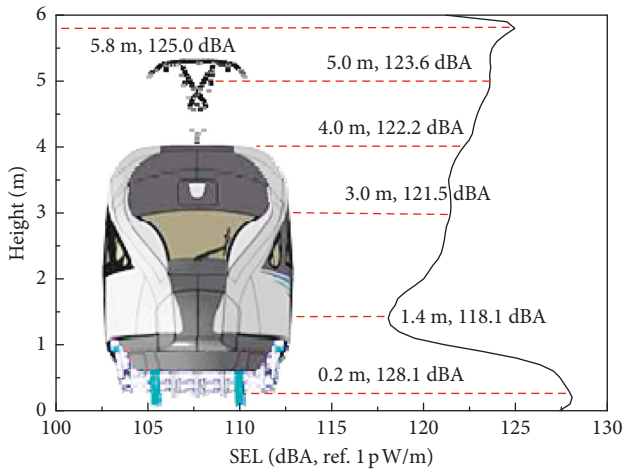


Figure 10: Vertical distribution of the exterior noise sources of a high-speed train running at 350 km/h (500–5000 Hz).

vertical direction for the train running at 350 km/h. The frequency contribution rates are calculated by

$$\alpha_{i\text{th band},j\text{th height}} = \frac{10^{\left(\text{SEL}_{i\text{th band},j\text{th height}}/10\right)}}{\sum_{\text{bands}} 10^{\left(\text{SEL}_{i\text{th band},j\text{th height}}/10\right)}} \times 100\%, \quad (5)$$

where $\text{SEL}_{i\text{th band},j\text{th height}}$ is the SEL of the $i$th 1/3 octave band and the $j$th height.

As indicated in Figure 11(a), the exterior sources in the 1/3 octave bands centred at 500 Hz, 630 Hz, 4 kHz, and 5 kHz, relatively, have low SELs in the vertical direction, which can also be concluded from the results of the frequency contribution rate in Figure 11(b). However, at 0.2–0.5 m heights, there are obvious noise peaks in the 1/3 octave bands ranging from 500 Hz to 2 kHz, and the peak decreases as the frequency increases. This should be related to the directivity of the rolling noise.

Figure 12 shows the vertical distribution of the exterior noise sources of a high-speed train at different speeds.

It can be seen from Figure 12 that the vertical SEL of the exterior noise sources increases with an increasing train speed. However, the increase rates at different heights vary. When the speed increases from 200 km/h to 350 km/h, the SELs at 0.2 m, 1.4 m, and 5.8 m above the railhead increase by 6.2, 8.2, and 8.1 dBA, respectively. Therefore, as the speed increases, the SEL in the carbody region increases more than that in the bogie region.

## 4. Simulation and Prediction of the Exterior Noise of a High-Speed Train

*4.1. Numerical Model of the Exterior Noise.* The numerical model of the exterior noise of the high-speed train is established based on the method of ray acoustics by using the software LMS Virtual Lab Acoustics. Figure 13 shows the exterior noise simulation model of the high-speed train. The simulation model considers the acoustic boundary of the carbody, the sound absorption of the track, the sound diffraction in propagation, and the characteristics of different sound sources. The characteristics of different sound sources include their locations, spectrums, and amplitudes.

The track surface of the viaduct is 10.5 m above the ground; therefore, the ground reflection is ignored in the model. The analysed frequency range ranged from 500 Hz to 5 kHz with 1/3 octave bands.

Table 2 shows the acoustic impedances in the direction normal to the carbody materials.

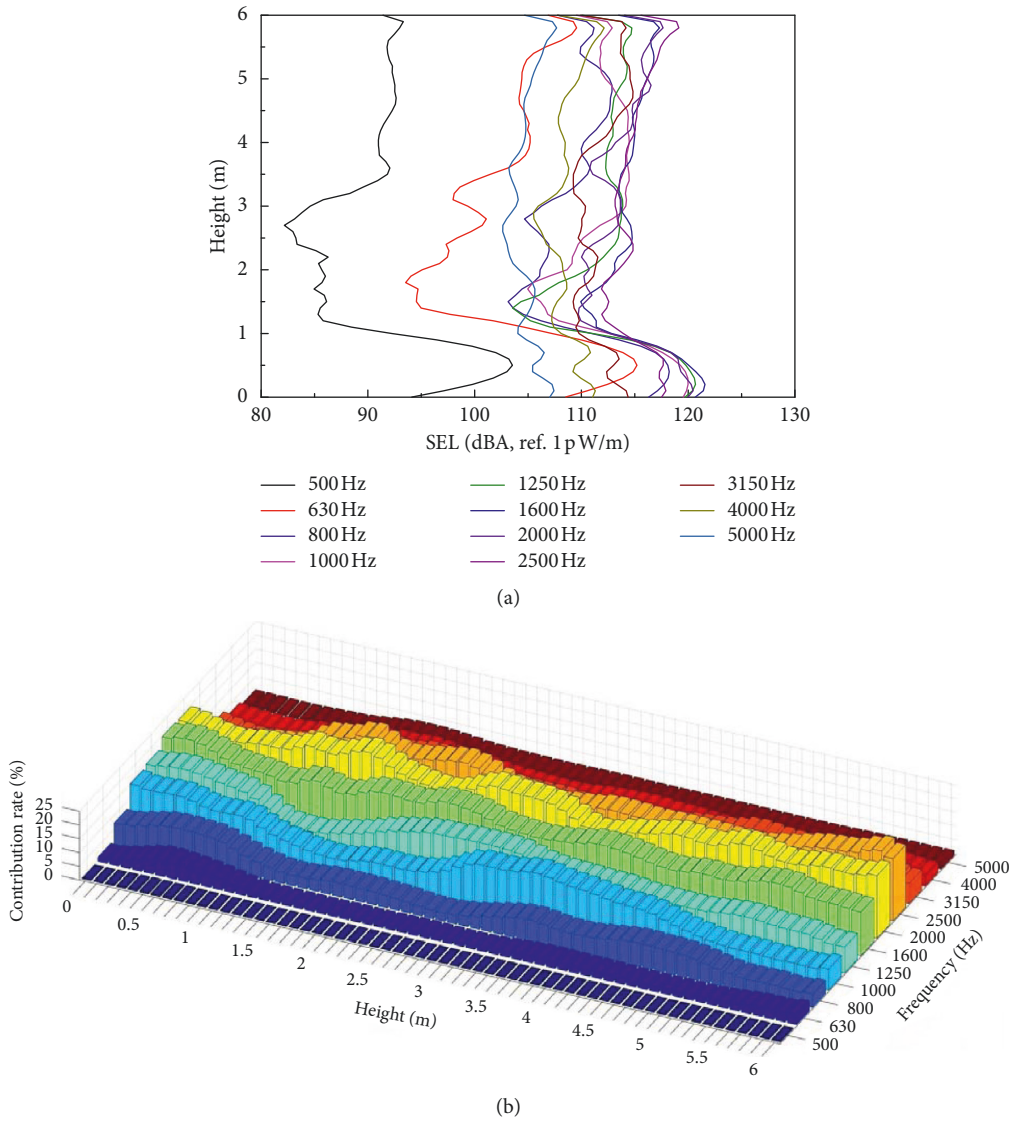


Figure 11: Frequency characteristics of the exterior noise sources in the vertical direction (350 km/h). (a) Frequency distributions. (b) Frequency contribution rates.

Table 3 shows the sound absorption of the slab track.

According to the division regions of the whole high-speed train in Figure 7, there are eight kinds of regions: pantograph, roof region, train head, train rear, coach centre, bogie, lower region, and intercoach. First, for each coach (the train consists of eight coaches), the sound power of the above eight kinds of regions is obtained by integrating the sound intensity over the area of each region. Subsequently, the sound power of each region is divided into a number of monopole sources according to the region area.

Table 4 shows the numbers and locations of the equivalent noise sources. According to the number and area division of the equivalent sound sources, they are uniformly distributed in the horizontal direction. Each equivalent noise source is close to the locations where there are components of the train that are radiating noise.

*4.2. Exterior Noise Prediction and Validation.* Figure 14 shows the time histories of the predicted and measured pass-by noise for the train running at 350 km/h. In addition, Figure 15 shows their frequency characteristics.

From Figures 14 and 15, it can be seen that the predicted results of the sound pressure level follow almost the same trend as the measurement results. However, the predicted $L_{\mathrm{Aeq,Tp}}$ results at 7.5 m and 25 m are 1.4 dBA and 1.3 dBA lower, respectively, than the measured results. The simulation results at the two points give an underestimate at high frequencies compared with the single microphone measurements. One of the reasons is that the simulated frequency range spans only from 500 Hz to 5 kHz in 1/3 octave bands because of the sound resolution limitation of the noise source identification results, whereas the pass-by noise measurement frequency range spans from 31.5 Hz to 8 kHz in 1/3 octave bands. However, this is not the key

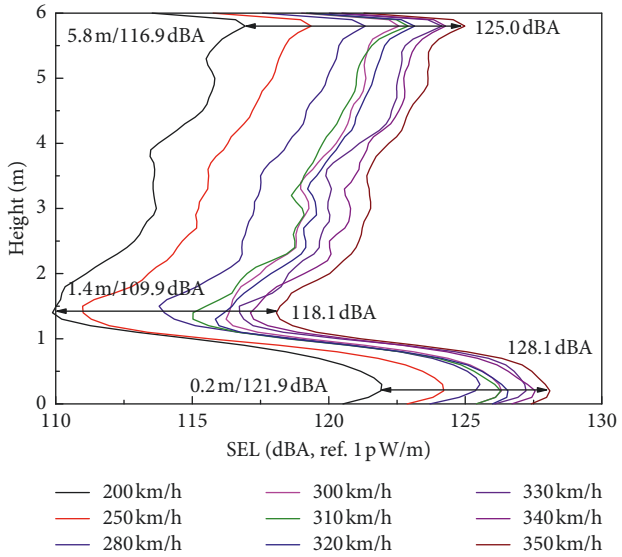


Figure 12: Vertical distribution of the exterior noise sources at different speeds (500–5000 Hz).

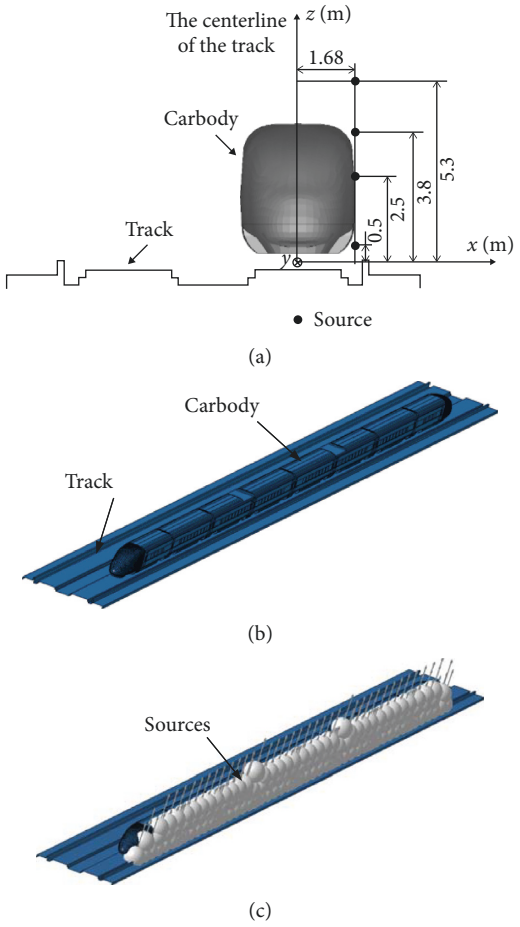


Figure 13: The exterior noise simulation model of a high-speed train. (a) Details of the source positions. (b) Whole train model. (c) Whole train model with sound sources.

Table 2: Acoustic impedances in the normal direction of the carbody materials (nominal values).

| Structure | Material | Acoustic impedance ($10^6$ MKS rayls) |
|---|---|---|
| Carbody | Aluminium | 17.1 |
| Window | Glass | 13.1 |

Table 3: Sound absorption of the slab track (nominal values).

| $f$ (Hz) | 125 | 250 | 500 | 1000 | 2000 | 4000 |
|---|---|---|---|---|---|---|
| $\alpha$ | 0.01 | 0.01 | 0.015 | 0.02 | 0.02 | 0.02 |

Table 4: The numbers and heights of equivalent noise sources.

| Area division of carbody surface | Source height above the rail (m) | Number of equivalent sources | Equivalent source height above the rail (m) |
|---|---|---|---|
| Pantograph | 3.4–6.0 | 2 | 5.3 |
| Roof region | 3.4–4 | 34 | 3.8 |
| Train head | 1–4 | 2 | 2.5 & 0.5 |
| Train rear | 1–4 | 2 | 2.5 & 0.5 |
| Coach centre | 1–3.4 | 36 | 2.5 |
| Bogie | 0–1 | 16 | 0.5 |
| Lower region | 0–1 | 36 | 0.5 |
| Intercoach | 0–4 | 7 | 0.5 |

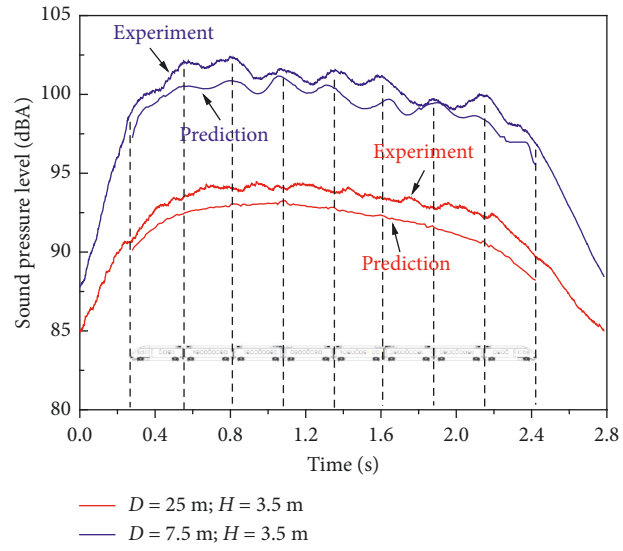


Figure 14: Time histories of the predicted and measured pass-by noises at 350 km/h.

factor since the high-frequency noises are dominant (as indicated in Figure 15). The main reason is probably the underestimation of high-frequency source contributions due to the characteristics of the microphone array, although the fact that track noise and bridge noise are ignored may also be a factor. This is an indication that the present predicted model needs to be further improved. Since the differences between the predicted and measured $L_{Aeq,Tp}$ results are only around 1 dBA and their frequency curves are well matched, the exterior noise prediction model established in this study is reliable and effective.

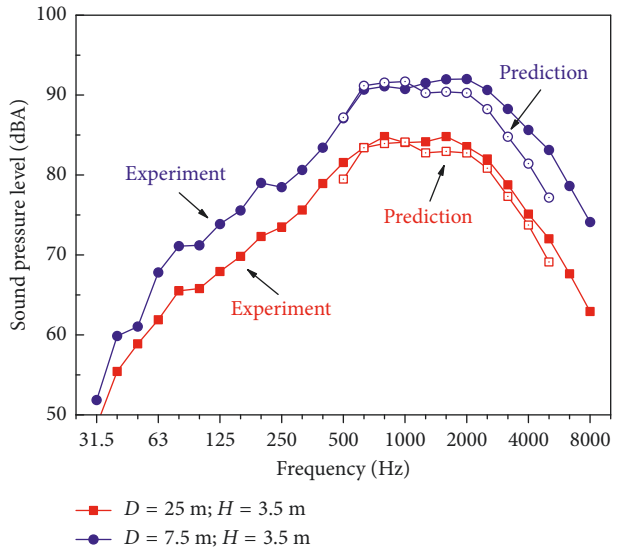


Figure 15: Frequency characteristics of the predicted and measured pass-by noises at 350 km/h.

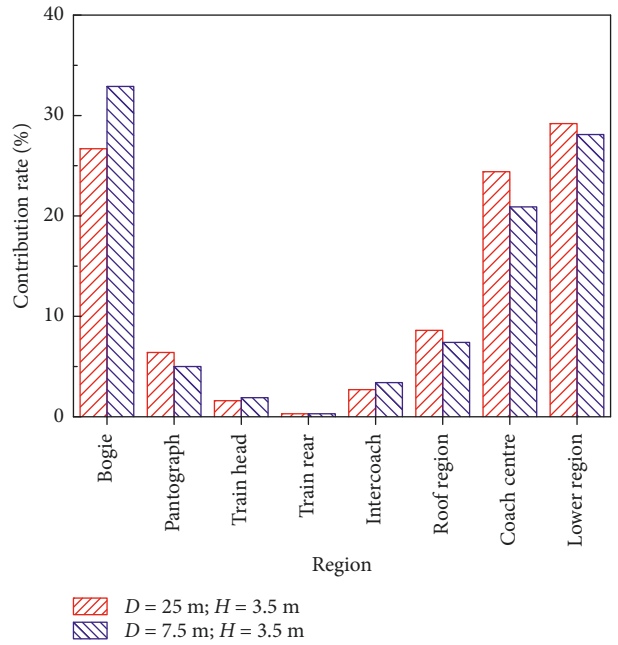


Figure 16: Contribution rates of the exterior sound sources to the pass-by noise (350 km/h).

## 5. Contribution Analysis of the Exterior Noise Sources to the Pass-By Noise

*5.1. Contribution Analysis of the Exterior Noise Sources from the Different Regions to the Pass-By Noise.* Based on the simulation model established in the above section, Figure 16 shows the contribution rates of the exterior sound sources to the pass-by noise at 7.5 m and 25 m away from the centreline of the track.

It can be seen from Figure 16 that when the high-speed train runs at 350 km/h, whether at a distance of 7.5 m or 25 m, the sources in the bogie, coach centre, and lower region are the three of the highest contributors. Their contribution rates are 32.9 %, 20.9 %, and 28.1 %, respectively, at 7.5 m and 26.7 %, 24.4 %, and 29.2 %, respectively, at 25 m. Here, the results come to almost the same conclusions with Figure 8, which due to the acoustic powers of the equivalent sources in the simulation model are set to match the measured results. The contribution of the bogie noise to the pass-by noise decreases from 7.5 m to 25 m, while the contributions of the coach centre and lower region increase. When the distance from the surface of the train grows, the contributions of the carbody sources, including the lower region, coach centre, roof region, and the pantograph, become higher. Meanwhile, the contributions of the sources in the bogie and train head become smaller. This is due to the directivities of the sources in different regions. The contribution of the sources in the train rear is very small and can be neglected.

*5.2. Influence of Train Speed on the Contribution Characteristics of the Sources.* Figure 17 shows the contribution rates of the exterior sound sources to the pass-by noise at different speeds at distances 7.5 m and 25 m.

It can be seen from Figure 17(a) that for the three most significant exterior noise sources, the contributions of the bogie and lower region decrease with the train speed, while those of the coach centre increase. The reason is indicated in Section 3.3. The contribution of the remaining regions of the exterior sound sources is less than 10 %, and the contribution change is not obvious with the changing speed. The contributions of the pantograph and train head increase a little with the increasing speed.

When the distance from the track centreline changes from 7.5 m to 25 m, as shown in Figure 17(b), the contributions of the exterior sound sources to the pass-by noise at different speeds does not change. However, the source contribution of the bogie at 25 m is lower than that at 7.5 m at different speeds, while the source contributions of the coach centre and lower region at 25 m are higher than those at 7.5 m at different speeds.

*5.3. Influence of Different Sound Sources on the Pass-By Noise.* According to the above analysis, to control the pass-by noise of a high-speed train, we should pay more attention to the exterior noise sources coming from the bogie, coach centre, and lower region. The influence of different sound sources on the pass-by noise is investigated by constructing the amplitude frequency curves, varying the sound power levels in steps from 1 to 5 dBA for each exterior sound source in different regions.

Figure 18 shows the influence of different sound sources on the pass-by noise.

The influence of different sound sources on the pass-by noise can be expressed by a quadratic curve as

$$L_{\mathrm{Aeq,Tp}}(x) = ax^2 + bx + L_{\mathrm{Aeq,Tp0}}, \quad x = -5, -4, -3, \ldots 5, \tag{6}$$

where $a$ and $b$ are coefficients, $x$ is the step of the sound power level change, and $L_{\mathrm{Aeq,Tp0}}$ is the value of $L_{\mathrm{Aeq,Tp}}$ at $x = 0$.

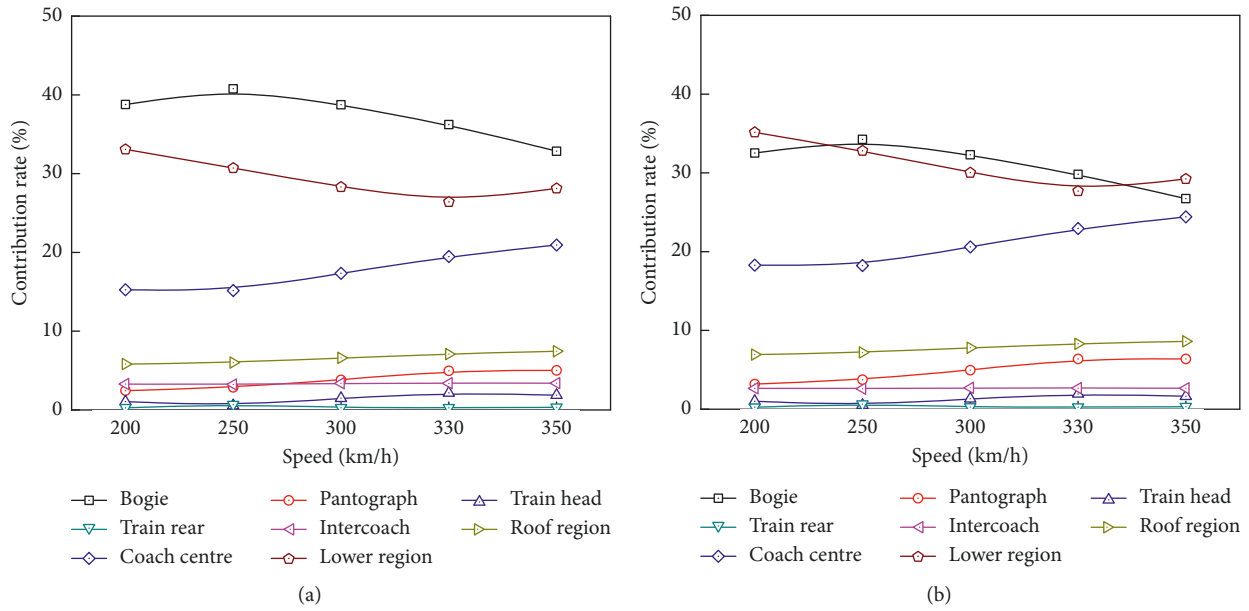


FIGURE 17: Contribution rates of the exterior sound sources to the pass-by noise at different speeds. (a) 7.5 m from the centreline of the track; (b) 25 m from the centreline of the track.

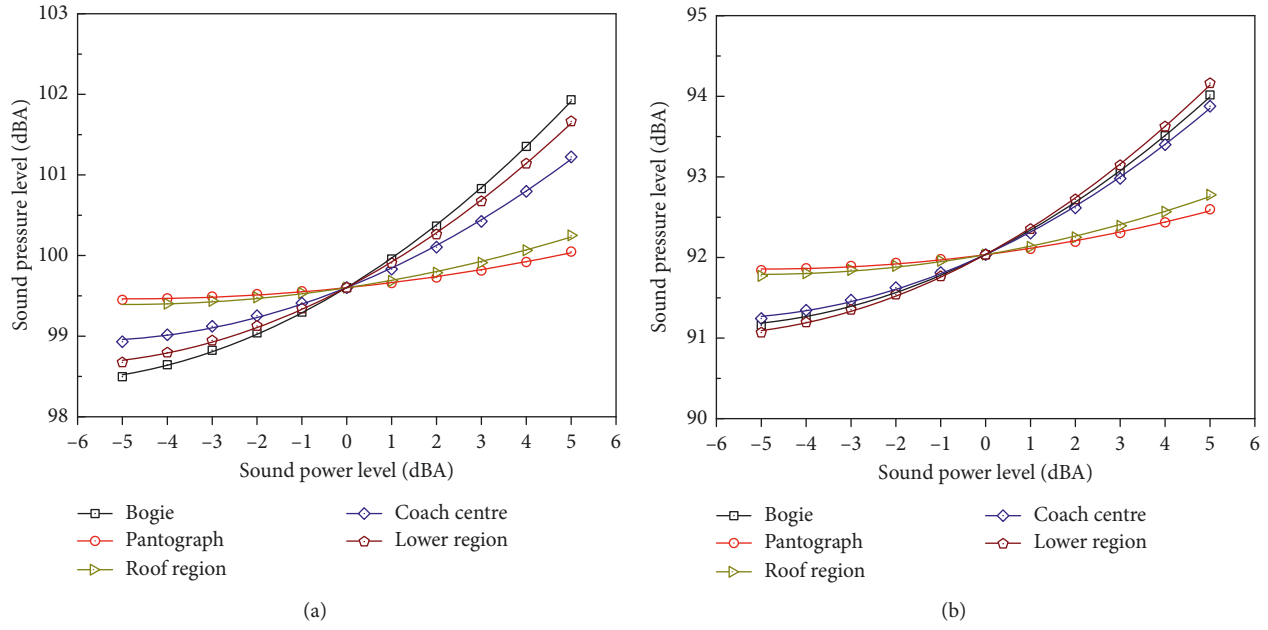


FIGURE 18: Influence of different sound sources on the pass-by noise. (a) 7.5 m from the centreline of the track; (b) 25 m from the centreline of the track.

Table 5 shows the fitting results, in which $R^2$ is the corresponding correlation coefficient.

It can be seen from Figure 18(a) that when the sound source level in the bogie is increased by 5 dBA, the pass-by noise level increases by approximately 2.3 dBA. When the sound source level in the bogie is reduced by 5 dBA, the pass-by noise level decreases by approximately 1.1 dBA. Therefore, the increase of the pass-by noise level, caused by the increase of the noise source levels in bogie, is greater than the decrease of the pass-by noise level, caused by the same magnitude decrease of the noise source levels in the bogie. The other noise sources show similar behaviour. Although reducing the noise source level of any region has a limited effect on the pass-by noise, the pass-by noise can increase significantly if the sound source levels, especially in the bogie, coach centre, and lower region, are not well controlled.

When the distance increases from 7.5 m to 25 m, as shown in Figure 18(b), the influences of the sound sources in the bogie, the coach centre, and lower region on the pass-

Table 5: Fitting results for the pass-by noise under different noise control values.

| | Bogie | | Pantograph | | Roof region | | Coach centre | | Lower region | |
|---|---|---|---|---|---|---|---|---|---|---|
| | 7.5 m | 25 m | 7.5 m | 25 m | 7.5 m | 25 m | 7.5 m | 25 m | 7.5 m | 25 m |
| $A$ | 0.3395 | 0.2807 | 0.0571 | 0.0722 | 0.0838 | 0.0964 | 0.2237 | 0.2580 | 0.2941 | 0.3048 |
| $B$ | 0.0245 | 0.0221 | 0.0059 | 0.0074 | 0.0084 | 0.0096 | 0.0190 | 0.0210 | 0.0227 | 0.0232 |
| $R^2$ | 0.9998 | 0.9996 | 0.9969 | 0.9972 | 0.9974 | 0.9977 | 0.9992 | 0.9994 | 0.9996 | 0.9997 |

by noise are getting close to each other. As indicated in Table 5, at 7.5 m, the influences of the different sound sources on the pass-by noise from the highest to lowest are the bogie, lower region, coach centre, roof region, and pantograph. While at 25 m, the sound source in the lower region has the highest effect on the pass-by noise. As the distance increases, the difference of the influences of the sound sources in the bogie, coach centre, and lower region on the pass-by noise decreases.

## 6. Conclusions

This paper presents a detailed investigation into the contributions of different sound sources to the exterior noise of a high-speed train both experimentally and by simulations. The measurement points of pass-by noise were arranged according to the international standard ISO 3095. The noise source identification was conducted using a 78-channel wheel microphone array, and the method of rail vehicle moving source beamforming was used for the source analysis. A numerical model of the exterior noise of the high-speed train was established based on the method of ray acoustics by using the software LMS Virtual Lab Acoustics, and the inputs come from the array measurements. The following conclusions can be drawn:

(1) When the train was running at 350 km/h, the sound pressure levels almost decrease from the first intercoach to the train tail during the pass-by time. The pass-by noise is dominated by high frequencies, especially in the 1/3 octave bands centred above 500 Hz. The sources with the highest levels are located at bogie and pantograph regions. For different coaches of the high-speed train, the highest aerodynamic noise levels are at the front coach, whereas relatively low aerodynamic noise levels occur at the end coach.

(2) The contributions of the noise sources in the carbody region on the pass-by noise appear to increase with the increasing distance of the pass-by noise measurement positions, while those in the bogie and train head decrease. The source contribution rates of the bogie and lower region decrease with the increasing train speed, while those of the coach centre increase. At 25 m from the track central line, the influences of the different noise sources on the pass-by noise, from the highest to lowest, are those in the lower region, bogie, coach centre, roof region, and pantograph.

(3) Although reducing the noise source level of any region has limited effects on the pass-by noise, it can increase significantly if the noise source levels, especially in the bogie, coach centre, and lower region, are not well controlled.

It is consistent with previous studies that the dominant sources are located at bogie and pantograph regions. For the results of source contribution, they are merely based on the beamforming results so that the resolution of the microphone array is very important. Different high-speed trains, different lines, different microphone arrays, and different algorithms can make differences in the results. Hence, some limitations of this study and further works that need to be done in the future are as follows:

(1) In this paper, because the source identification result is mainly concerned with the train itself, the contributions of the rail, the track, and the bridge are not discussed.

(2) According to the maximum sidelobe levels for the microphone array used in this measurement, source contribution from carbody to the total sound power may be overestimated. It needs to be further investigated.

## Data Availability

The data used to support the findings of this study are available from the corresponding author upon request.

## Conflicts of Interest

The authors declare that they have no conflicts of interest.

## Acknowledgments

This work was supported by the National Key R&D Program of China (nos. 2016YFE0205200, 2016YFB1200506-08, and 2016YFB1200503-02) and the National Natural Science Foundation of China (nos. U1434201 and 51475390). The authors are grateful to Bin He, Mu-xiao LI, Zhi-hui LI, and Mou-kai Liu (Southwest Jiaotong University, China) and Zhigang Chu (Chongqing University, China) for their assistance in this study.

## References

[1] X. S. Jin, "Key problems faced in high-speed train operation," *Journal of Zhejiang University Science A*, vol. 15, no. 12, pp. 936–945, 2014.

[2] N. I. Ivanov, I. S. Boiko, and A. E. Shashurin, "The problem of high-speed railway noise prediction and reduction," *Procedia Engineering*, vol. 189, pp. 539–546, 2017.

[3] B. Schulte-Werning, K. Jäger, R. Strube, and L. Willenbrink, "Recent developments in noise research at Deutsche Bahn (noise assessment, noise source localization and specially monitored track)," *Journal of Sound and Vibration*, vol. 267, no. 3, pp. 689–699, 2003.

[4] Y. Wakabayashi, T. Kurita, H. Yamada, and M. Horiuchi, "Noise measurement results of Shinkansen high-speed test train (FASTECH360S,Z)," *Notes on Numerical Fluid Mechanics*, vol. 99, pp. 63–70, 2008.

[5] F. Poisson, P. E. Gautier, and F. Letourneaux, "Noise sources for high speed trains: a review of results in the TGV case," *Noise and Vibration Mitigation for Rail Transportation Systems*, vol. 99, pp. 71–77, 2008.

[6] C. Mellet, F. Létourneaux, F. Poisson et al., "High-speed train noise emission: latest investigation of the aerodynamic/rolling noise contribution," *Journal of Sound and Vibration*, vol. 293, no. 3–5, pp. 535–546, 2006.

[7] K. Nagakura, "Localization of aerodynamic noise sources of Shinkansen trains," *Journal of Sound and Vibration*, vol. 293, no. 3–5, pp. 547–556, 2006.

[8] B. He, X. B. Xiao, Q. Zhou et al., "Investigation into external noise of a high-speed train at different speeds," *Journal of Zhejiang University Science A*, vol. 15, no. 12, pp. 1019–1033, 2014.

[9] H. M. Noh, "Noise-source identification of a high-speed train by noise source level analysis," *Proceedings of the Institution of Mechanical Engineers Part F: Journal of Rail and Rapid Transit*, vol. 231, no. 6, pp. 717–728, 2017.

[10] C. Talotte, P. van der Stap, M. Ringheim, M. Dittrich, X. Zhang, and D. Stiebel, "Railway source models for integration in the new European noise prediction method proposed in Harmonoise," *Journal of Sound and Vibration*, vol. 293, no. 3–5, pp. 975–985, 2006.

[11] P. J. Remington, "Wheel/rail rolling noise I: theoretical analysis," *Journal of the Acoustical Society of America*, vol. 81, no. 6, pp. 1805–1823, 1987.

[12] D. J. Thompson and P. E. Gautier, "Review of research into wheel/rail rolling noise reduction," *Proceedings of the Institution of Mechanical Engineers, Part F, Journal of Rail and Rapid Transit*, vol. 220, no. 4, pp. 385–408, 2006.

[13] E. Zea, L. Manzari, G. Squicciarini, L. Feng, D. Thompson, and I. L. Arteaga, "Wavenumber-domain separation of rail contribution to pass-by noise," *Journal of Sound and Vibration*, vol. 409, pp. 24–42, 2017.

[14] D. J. Thompson, G. Squicciarini, J. Zhang et al., "Assessment of measurement-based methods for separating wheel and track contributions to railway rolling noise," *Applied Acoustics*, vol. 140, pp. 48–62, 2018.

[15] E. Latorre Iglesias, D. J. Thompson, and M. G. Smith, "Component-based model to predict aerodynamic noise from high-speed train pantographs," *Journal of Sound and Vibration*, vol. 394, pp. 280–305, 2017.

[16] J. Y. Zhu, Z. W. Hu, and D. J. Thompson, "Flow simulation and aerodynamic noise prediction for a high-speed train wheelset," *International Journal of Aeroacoustics*, vol. 13, no. 7-8, pp. 533–552, 2014.

[17] ISO (International Organization for Standardization), *Acoustics—Railway applications—Measurement of Noise Emitted by Railbound Vehicles*, ISO 3095:2013, Geneva, Switzerland, 2013.

[18] J. J. Christensen and J. Hald, *Technical Review Beamforming*, Bruel and Kjear, Nærum, Denmark, 2004.

[19] J. Hald, "Estimation of partial area sound power data with beamforming," in *Proceedings of Inter-Noise and Noise-Con Congress and Conference*, Rio de Janeiro, Brazil, August 2005.

[20] Z. G. Chu and Y. Yang, "Comparison of deconvolution methods for the visualization of acoustic sources based on cross-spectral imaging function beamforming," *Mechanical Systems and Signal Processing*, vol. 48, no. 1-2, pp. 404–422, 2014.

[21] Z. G. Chu, C. H. Chen, Y. Yang, and L. Shen, "Two-dimensional total variation norm constrained deconvolution beamforming algorithm for acoustic source identification," *IEEE Access*, vol. 6, pp. 43743–43748, 2018.